Remote Sensing of Environment 115 (2011) 2116–2125

Contents lists available at ScienceDirect

Remote Sensing of Environment

journal homepage: www.elsevier.com/locate/rse

Relating the X-band opacity of a tropical tree canopy to sapflow, rain interception and dew formation

Marc Schneebeli [a,c,*,1], Sebastian Wolf [b], Norbert Kunert [d], Werner Eugster [b], Christian Mätzler [c]

[a] EPFL, Environmental Remote Sensing Laboratory, Lausanne, Switzerland
[b] ETH Zurich, Institute of Plant, Animal and Agroecosystem Sciences, Zurich, Switzerland
[c] University of Bern, Institute of Applied Physics, Bern, Switzerland
[d] Max-Planck-Institute for Biogeochemistry, Department of Biogeochemical Processes, Jena, Germany

ARTICLE INFO

Article history:
Received 29 November 2010
Received in revised form 23 March 2011
Accepted 10 April 2011
Available online 10 May 2011

Keywords:
X-band
Tropics
Rain interception
Dew
Sapflow
Radiometry
Microwave techniques
Eddy covariance

ABSTRACT

During summer and autumn 2007, a 11 GHz microwave radiometer was deployed in an experimental tree plantation in Sardinilla, Panama. The opacity of the tree canopy was derived from incoming brightness temperatures received on the ground. A collocated eddy-covariance flux tower measured water vapor fluxes and meteorological variables above the canopy. In addition, xylem sapflow of trees was measured within the flux tower footprint. We observed considerable diurnal differences between measured canopy opacities and modeled theoretical opacities that were closely linked to xylem sapflow. It is speculated that dielectric changes in the leaves induced by the sapflow are causing the observed diurnal changes. In addition, canopy intercepted rain and dew formation also modulated the diurnal opacity cycle. With an enhanced canopy opacity model accounting for water deposited on the leaves, we quantified the influence of canopy stored water (i.e. intercepted water and dew) on the opacity. A time series of dew formation and rain interception was directly monitored during a period of two weeks. We found that during light rainfall up to 60% of the rain amount is intercepted by the canopy whereas during periods of intense rainfall only 4% were intercepted. On average, 0.17 mm of dew was formed during the night. Dew evaporation contributed 5% to the total water vapor flux measured above the canopy.

1. Introduction

1.1. Rain interception and dew formation

Tropical rain forests play a dominant role in the earth's water balance. An important fraction of the hydrological cycle amounts to rain water interception and its subsequent re-evaporation. According to Lawrence et al. (2007), transpiration is the dominant process of evapotranspiration with a contribution of 58%, followed by interception evaporation (33%) and soil evaporation (9%).

Rain interception is rather difficult to measure accurately. The most frequently used technique is the measurement of throughfall by setting up several rain-gages below the canopy and one or more above the canopy. The difference of the collected water is assumed to be withheld by the canopy. There are some major drawbacks to this method: Due to the complex structure of a forest canopy, the spatial variability of the throughfall is very large, hence numerous rain gages are needed in order to achieve representative and accurate sampling (Kimmins, 1973). Direct evaporation of intercepted rain water is another effect that cannot be tackled with the throughfall method, wherefore reliable measurements can only be conducted during night time.

A promising technique is the attenuation measurement of a 10 GHz signal over a horizontal path through a Douglas fir stand as reported in Bouten et al. (1991). They observed a distinct linear relation of the attenuated signal to intercepted rain. The authors then employed this attenuation method in several upcoming studies as a monitoring tool for water interception in forest canopies (Bouten et al., 1996; Vrugt et al., 2003). Czikowsky and Fitzjarrald (2009) reported on a new interception estimation technique that estimates the excess evaporation following rain events with eddy covariance flux measurements.

Recently, a global assessment of canopy interception from satellite data was published in Miralles et al. (2010). The authors used an analytical interception model (Valente et al., 1997) and fed it with satellite data of precipitation, lightning frequency and canopy fraction. It was found that the interception loss is sensitive to the rainfall volume, rain intensity and the forest cover. Some of these findings will be confirmed in the article at hand.

* Corresponding author at: EPFL, Environmental Remote Sensing Laboratory, Lausanne, Switzerland. Tel.: +41 21 69 35773.
E-mail address: marc.schneebeli@epfl.ch (M. Schneebeli).
[1] Now at: National Institute for Space Research (INPE), Center for Weather Forecast and Climate Studies (CPTEC), Cachoeira Paulista/SP, Brazil.

0034-4257/$ – see front matter © 2011 Elsevier Inc. All rights reserved.
doi:10.1016/j.rse.2011.04.016

Compared to intercepted rain, very little is known about the importance of dew formation and dew evaporation, most likely because no established measurement technique is available so far to measure the dew amount in a forest canopy. It is although known that dew not only promotes diseases of plant crops and is therefore an important parameter in agriculture (for tropical conditions see e.g. Holliday, 1980), according to Kabela et al. (2009), dew "also may contaminate remotely sensed measurements of important ecosystem variables such as soil moisture, land surface temperature, and vegetation biomass". Dew duration is relatively easy to measure by using electrical devices that change their resistance or capacity when becoming wet (Kidron et al., 1965; Noffsinger, 1965). However, methods for measuring dew amounts (e.g. weighing dew gages, weighing lysimeters) are limited and solely used for measurements close to the ground (Agam & Berliner, 2006).

1.2. Microwave properties of forest canopies

Microwave properties of tree canopies have been investigated for many years and good overviews over this research topic are given in Chukhlantsev (2006) and Pampaloni (2004). In contrast to the wealth of available information on radiometric forest properties like the emissivity of forests (e.g., Della Vecchia et al., 2007; Ferrazoli & Guerriero, 1996; Santi et al., 2009), canopy scattering (e.g., Karam et al., 1995) and canopy attenuation (e.g., Kurum et al., 2009), reports on measurements of diurnal variations in tree opacities as well as observations of tree opacities focusing on intercepted water are sparse. McDonald et al. (2002) reported on diurnal variations in the dielectric constant of the xylem and hypothesized a relation to the ascent of sap in the xylem. Satake and Hanado (2004) studied diurnal changes of the radar backscatter of tropical trees with the Ku-Band Radar of the TRMM satellite and concluded that the signal has a relation to dew formation. A large experiment on diurnal changes in the optical and microwave frequency range was reported in Way et al. (2004), although no evident conclusions on diurnal variations could be derived from their measurements at X-band frequencies.

With the launch of the SMOS satellite in November 2009, L-band attenuation through tree canopies is recently attracting interest and therefore several studies are being performed with L-band radiometers. A recent study by Guglielmetti et al. (2007) measured the L-band and X-band transmissivities of a deciduous forest site during a 4 month defoliation period. The main focus of this work was not on diurnal changes but they found out that leaves contribute more to the transmissivity at X-band than at L-band frequencies, leading to a stronger response to the defoliation of the canopy. In addition, it was shown that the transmissivity at both frequencies is related to the rain intensity. A similar experiment was conducted by Mätzler (1994b), who observed an individual beech tree during two years with several microwave radiometers that covered a frequency range from 1 to 100 GHz. A pronounced seasonal cycle caused by the foliation and defoliation of the tree was registered during this experiment.

In our study, the downwelling brightness temperature of a tropical tree canopy was measured with a ground deployed 11.4 GHz microwave radiometer that was looking up through the canopy. The objectives of these measurements were to test if the opacity of the tree canopy underlies a diurnal cycle and to relate the microwave signal to the amount of water deposited on the leaves. In Section 2, the microwave radiometer and the other instruments are described. Section 3 treats the different radiative transfer models that allow 1. to calculate the canopy opacity, 2. to model the effect of the temperature on the opacity and 3. to account for the radiative effect of wet leaves in the canopy. Furthermore, we also relate the sapflow in the tree to opacity of the tree. These findings were then applied to opacity time series in Section 4 and they allowed us to quantify the water amount of intercepted rain and dew formation in the canopy. Finally, in Section 5 we summarize and conclude on our findings.

2. Instruments and study site

2.1. Microwave radiometer

For this experiment, a single polarization microwave radiometer operating at a frequency of 11.4 GHz has been developed. The frequency selection was based on the availability of high-quality but still inexpensive receivers. From the point of view of the application there is nothing against this selection. For our purpose and in order to be deployed in a tropical environment, the instrument had to fulfill certain requirements. First of all, an instrument with automated internal calibration was needed, since tipping-calibration (Han & Westwater, 2000) is not possible below the canopy and manual calibration with hot/cold black-body loads not desirable. To achieve this, the instrument was equipped with a waveguide switch, switching every 5 s to an ambient load (internal termination load enclosed in a copper block). Every minute, additional 80 K noise from a solid state noise source was coupled in over a 20 dB cross coupler. Second, the instrument needed protection against tropical heat, high relative humidity, rain and insects. This was achieved by installing the radiometer together with the horn antenna in a sealed solid aluminum box. The radiation entered the box through a microwave transparent Styrofoam window. The Schottky diode detectors and the noise source, being the most temperature critical components, were enclosed in a solid aluminum block and attached to a Peltier element, capable of heating and cooling. The temperature of this block was stabilized to 26 °C such that the Peltier element had to cool during the day and to heat during the night, when we had high relative humidity. Finally, our system had built-in data acquisition and storage and was capable of unattended operation over several days. Data were taken every 100 ms and averaged over one full calibration cycle of 1 min.

The radiometer has two channels, both measuring at the same center frequency but one with 50 MHz and the other with 500 MHz bandwidth. The 50 MHz channel was built in the radiometer in order to mitigate possible radio frequency interferences (RFI) that are more likely for a wider bandwidth. Since the antenna could be adjusted to a position where no RFI was detected, the wider bandwidth was employed for all the measurements, resulting in an improved signal-to-noise ratio. The antenna we used is a rectangular horn with a beam width of about 15°. In addition to the microwave part, a thermal infrared radiometer (Everest 4000.5 GL) was installed in the box. More technical details on the radiometer system are found in Schneebeli et al. (2008).

The microwave radiometer was placed on the ground, looking upwards through the canopy under an elevation angle of 40°, measuring in horizontal polarization. A tarp, set-up above the instrument without interfering with the radiometer's line-of-sight, protected the antenna from becoming wet and therefore enabled us to conduct measurements during rain as well. Data were gathered from July to October 2007. Fig. 1 shows the instrument operating at the field site in Sardinilla.

2.2. Sapflow measurements

Continuous measurements of xylem sapflow were performed within the flux tower footprint using the thermal dissipation method by Granier (1985). The sapflow sensors consisted of two cylindrical probes that were embedded into the tree stem (0–20 mm below cambium) with a vertical distance of 10–15 cm between both probes. Two sensors were installed on each of the 5 trees measured, at 130 cm height (DBH) on the southern and northern side of the trees. A Styrofoam box combined with reflective foil and a plastic cover reduced thermal influences and provided rain shelter. Voltage output of the thermocouple were measured every 30 s and 15 min averages were stored on CR800 and CR1000 data loggers, and AM16/32 and AM416 multiplexer (Campbell Scientific, Logan, USA). Sap flux

Fig. 1. The microwave radiometer deployed in the field.

velocity (m/h) was calculated from differences in voltage using the calibration equation determined by Granier (1987). Further details on the measurements and the calculation of sapflow are given in Kunert et al. (2010).

2.3. Eddy covariance flux measurements

Continuous eddy covariance flux measurements were conducted at 20 Hz atop a 15 m aluminum triangle tower using an open path infrared gas analyzers (IRGA, Li-7500, LI-COR, Lincoln, USA) and a three-dimensional sonic anemometer (CSAT3, Campbell Scientific, Logan, USA). An industry grade embedded box computer (Advantech ARK-3381, Taipei, Taiwan) running a Debian based Linux operating system (Knoppix 4.0.2, Klaus Knopper, Schmalenberg, Germany) was used for the flux data acquisition. Raw data were processed to half-hourly averages using the in-house eddy covariance software eth-flux (ETH Zurich, Grassland Sciences Group) and the equation

$$F = p_a \overline{w'c'} \tag{1}$$

where F denotes the vertical water vapor flux, p_a the air density, w the vertical wind speed, c the water vapor concentration, the overbar the temporal averaging (30 min) and primes the variations from the mean. During post-processing, fluxes were corrected for damping loss (Eugster & Senn, 1995) and density fluctuations (Webb et al., 1980).

2.4. Meteorological and leaf area measurements

Additional meteorological measurements included air temperature and relative humidity (MP100A, Rotronic, Bassersdorf, Switzerland), and precipitation (10116, TOSS, Potsdam, Germany). Meteorological measurements were conducted at 10 s and stored as half-hourly averages (sums for precipitation) using a CR23X data logger (Campbell Scientific, Logan, USA). The leaf area index (LAI) of the canopy was determined with hemispherical photography and the software 'Gap Light Analyzer' (© Simon Fraser University, Institute of Ecosystem Studies, BC).

Specific leaf area (SLA in $cm^2\ g^{-1}$) was estimated for trees equipped with sapflow sensors. For each tree five sun leaves and five shade leaves were collected and scanned with a commercial USB-scanner. Leaf surface area was determined from the images using Win Folia 5.1 a (Rgent Instruments Inc., Quebec, Canada). Leaves were dried for 3 days at 70 °C and weighed. We calculated SLA as the ratio of leaf surface to leaf dry mass.

2.5. Study site

The experiment was conducted near the village Sardinilla, Panama (9°19′N, 79°38′W), in an experimental biodiversity plantation (Potvin & Dutilleul, 2009). The canopy under observation consisted of *Anacardium excelsum*, *Tabebuia rosea* and *Hura crepitans*. The trees had an age of about 7 years and an average height of 8 m. Mean SLA of the studied species and trees were 88, 96 and 138 $cm^2\ g^{-1}$, respectively (Kunert, unpublished data). Our experiment took place within the wet season (May to November) that is characterized by about 205 mm rainfall per month. The site receives 2289 mm annual precipitation and the temperature is relatively constant throughout the year with an annual mean of 25.2 °C.

The leaves of *A. excelsum* are simple, alternative and relatively large. Leaf length is between 15 and 35 cm, leaf width is between 5 and 15 cm. The leaves have no stipules, are obovate–oblong in outline with a rounded apex. The texture is glabrous and coriaceous. The species has a rounded and dense crown (Fournier, 2003).

The leaves of *H. crepitans* are simple and have long petioles. The leaves are ovate with cordate-shaped apex and a round base. The margin of the leaves is denticulated and the stipules are lanceolate or triangular. Leaves are between 4 and 16 cm long and equal in width. The texture is glabrous. The crown of *H. crepitans* is wide and the horizontal spreading branches have hanging twigs (Sandi & Flores, 2003).

The leaves of *T. rosea* are decussate, compound, digitate and long petiolate. Each leaf consists out of five leaflets that differ in size, with the leaflet in the middle being the largest. The shape ranges between elliptic–oblong, obovate and oblong–ovate. The apex is acute or acuminate, has an entire margin, and an obtuse base. The leaf surface can be glabrous or rough on both the upper and lower surfaces. The leaflets are between 6 and 20 cm long and between 3 and 10 cm wide. The crown of *T. rosea* is wide, well stratified with a few thick branches that grow irregular and horizontal (Flores & Marin, 2003).

3. Method

3.1. Canopy opacity from measurements

According to Mätzler (1994b), the canopy transmissivity t_c can be expressed with the following equation:

$$t_c = \frac{T_c - T_{b,in}}{T_c - T_{b,\mathrm{sky}}} \tag{2}$$

T_c is hereby the physical canopy temperature measured with the infrared radiometer, $T_{b,in}$ is the brightness temperature measured with the microwave radiometer and $T_{b,\mathrm{sky}}$ is the brightness temperature emitted from the sky. This formula is valid if one of two possible conditions is fulfilled: (1) if the reflectivity of the canopy is zero or (2) if the ground temperature is equal to T_c and the emissivity of the ground is 1. For details the reader is referred to Mätzler (1994b). Since our trees are relatively small, it is likely that condition (2) is true and that Eq. (2) is therefore valid. The effective opacity is obtained with the Beer–Lambert law,

$$\tau_{\mathrm{meas}} = -ln(t_c). \tag{3}$$

The subscript 'meas' was added to τ to indicate that this opacity is considered as measured quantity. As stated in Mätzler (1994b), this law is only valid for homogeneous media: In a canopy, where the transmissivity within the beam of a radiometer varies due to gaps between branches and leaves, the mean opacity is higher than what is obtained with Eq. (3). Since we observed a relatively dense canopy (LAI ≈ 3.5), where the spatial inhomogeneity is expected to be small, we neglected this effect.

What cannot be measured with this configuration is the sky radiation $T_{b,\mathrm{sky}}$, wherefore this contribution needs to be modeled. The

solution of the radiative transfer equation for a non-scattering atmosphere (e.g. Janssen, 1993) is used to calculate the incoming brightness temperature on the ground:

$$T_{b,\mathrm{sky}} = T_c e^{-\tau(s)} + \int_0^{\infty} \left(\gamma_a^{\mathrm{dry}}(s') + \gamma_a^{\mathrm{rain}}(s')\right) T(s') e^{-\tau(s')} ds'. \quad (4)$$

In the above equation, $T_c \approx 3$ K is the cosmic microwave background, $\tau(s)$ is the opacity along the path through the atmosphere s, $\gamma_a^{\mathrm{dry}}(s)$ and $\gamma_a^{\mathrm{rain}}(s)$ are the absorption coefficients for the dry atmosphere and the rain respectively and $T(s)$ denotes the temperature profile.

We assume $\gamma_a^{\mathrm{dry}}(s)$ to decrease exponentially with height. Therefore, the height profile of $\gamma_a^{\mathrm{dry}}(s)$ can be written as

$$\gamma_a^{\mathrm{dry}}(z) = \gamma_a^{\mathrm{dry}}(0) e^{-z/z_0^{\mathrm{dry}}} \quad (5)$$

where z_0^{dry} denotes the scale height and $z = s/cos(\theta)$ is the height above the ground with the zenith angle θ.

In addition, $T(s)$ is assumed to decrease linearly with height while $\gamma_a^{\mathrm{rain}}(s)$ is assumed to be equal to its surface value $\gamma_a^{\mathrm{rain}}(0)$ between the rain layer height z_0^{rain} and the surface. Everywhere else we set $\gamma_a^{\mathrm{rain}}(s) = 0$. Above z_0^{rain} we therefore have only the cosmic microwave background and the thermal emission from the dry atmosphere that contribute to the downwelling brightness temperature. The analytic model developed in Schneebeli and Mätzler (2011) can be used to calculate the brightness temperature T_b^{dry} intercepted at height z_0^{rain} as a function of the temperature on the ground T_g, the temperature gradient of the troposphere Γ, the height of the tropopause z_p, the scale height z_0^{dry}, the surface value of the absorption coefficient $\gamma_a^{\mathrm{dry}}(0)$ and the zenith angle θ. Below z_0^{rain} the total absorption coefficient profile and the temperature profile need to be discretized such that Eq. (4) can be solved numerically. The cosmic microwave background T_c is thereby exchanged with the already obtained T_b^{dry}.

For our simulations, the height of the tropopause z_p was set to 15 km and Γ to -6.5 K/km. With T_g, as well as the pressure and RH measured on the ground serving as input to the microwave absorption model of Rosenkranz (1998), $\gamma_a^{\mathrm{air}}(0)$ can be determined. Similarly, $\gamma_a^{\mathrm{rain}}(0)$ is calculated from the rain intensity measured on the ground by using the model of Liebe et al. (1993). Finally, adequate values for z_0^{rain} and z_0^{dry} had to be found. We found the best agreement between modeled brightness temperatures and measurements made above the canopy during clear-sky conditions with $z_0^{\mathrm{dry}} = 4$ km (see Fig. 3).

Usually, the rain layer height z_0^{rain} is parameterized with the height of the melting layer h_m, i.e. the 0 °C barrier of the atmosphere. In the tropics, this barrier is found around 4000 m, but it was pointed out in Czekala et al. (2001) that for heavy convective situations, as they predominantly occurred in the present study, the true rain layer height is no longer of importance, because of the three-dimensional structure of the rain fields. A simplified model that takes the spatial extent of the rain cells into account was therefore developed: The horizontal length of the rain field l_r was determined from the duration of the individual rain event t_r and the average wind speed of the event v_r with $l_r = v_r t_r$. Fig. 2 illustrates the situation of the radiometer being inside of a rain cell that was approaching the radiometer from ahead. From this figure it is seen that the rain layer height can be calculated as

$$z_0^{\mathrm{rain}} = tan(\theta)(l_r - t_e v_r) \quad (6)$$

where t_e is the elapsed time since the beginning of the rain event. If the rain cell is approaching the radiometer from behind, z_0^{rain} is calculated as

$$z_0^{\mathrm{rain}} = tan(\theta)(t_e v_r). \quad (7)$$

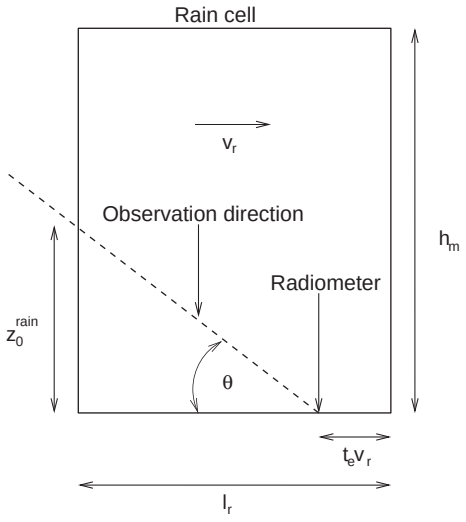

Fig. 2. Sketch of the radiometer located within a rain cell of limited vertical extent. The denotations are defined in the text.

The above equations are only true if $t_e v_r$ is smaller than l_r. For the case of a rain cell approaching from the side, we have to assume that both sides of the rain field have length l_r and that the radiometer is located in the middle of the field. This leads to

$$z_0^{\mathrm{rain}} = tan(\theta)(l_r / 2). \quad (8)$$

The melting layer height $h_m = (0°C + T_g)/\Gamma$ is used instead of z_0^{rain} where z_0^{rain} exceeds h_m. The three different cases were distinguished with the wind direction measurements. There is also a contribution from the rain when the radiometer is not located within the cell but the radiometer beam captures radiation from the remote rain field. This contribution is not modeled because information on the intensity of the distant rain field is not available. This modeling approach might appear like a strong simplification, but it was found that $T_{b,\mathrm{sky}}$ modeled with this method is consistent with brightness temperature measurements that were made above the canopy during rainfall (see the comparison shown in Fig. 3). Without considering the three dimensional structure of the rain fields the modeled radiation would be largely too high.

One must be aware that the estimation of z_0^{rain} introduces ambiguities in the estimation of $T_{b,\mathrm{sky}}$ during rainfall. On the other hand, the impact of $T_{b,\mathrm{sky}}$ on the canopy opacity is relatively small: An underestimation of $T_{b,\mathrm{sky}}$ of 20 K results in an opacity error of about 4% only. Despite the fact that the agreement between the modeled and measured brightness temperature is relatively good in the example shown in Fig. 3, one must be aware that a direct measurement with a second radiometer above the canopy would lead to more trustful results. For example, the contribution of clouds cannot be taken into account with our model and it is therefore expected that opacity errors exist during overcast non-rainy situations. Another potential error source is the spatial variability of precipitation (see e.g., Moreau et al., 2009): within a few hundred meters, the rain intensity can vary significantly, which also introduces opacity errors since the radiometer is looking into a distant atmosphere. The fact that rain intensity data with a temporal resolution of 1 min are averaged onto a half an hour time grid for the calculation of $T_{b,sky}$ might however mitigate this error source.

3.2. Canopy opacity model

For the interpretation of our measurements we incorporated an effective medium canopy opacity model of leaves, that treats

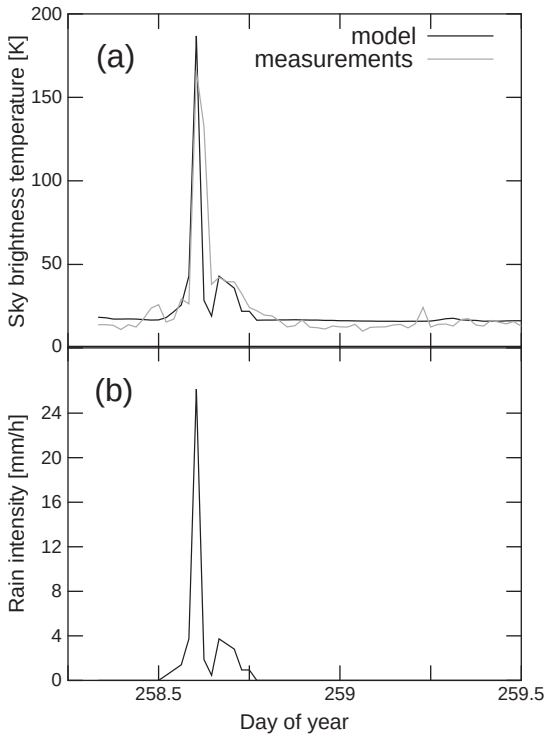

Fig. 3. a) Time series of the modeled microwave brightness temperature (11.4 GHz) of the sky at an elevation angle of 40° (black line) together with the measurements made above the canopy (gray line). b) Time series of the rain intensity measured with a tipping bucket rain gage.

scattering with a geometrical optics approach. It was described in Wegmüller et al. (1995) and is written as

$$\tau_{\text{temp}} = A_p \cdot \text{LAI} \cdot kd\epsilon_l'' \frac{1}{cos\theta} t_l + \tau_b. \quad (9)$$

The subscript 'temp' was added to τ in order to emphasize that in the forthcoming treatment all model parameters except the temperature are kept constant. In contrast to the original model, we added a constant opacity τ_b that takes into account the opacity contribution from the branches and the stem. In the above equation, A_p denotes a geometrical factor we set to 1 (Wegmüller et al., 1995), the leaf area index is set to LAI = 3.5, $k = 2\pi/\lambda$ is the wave number, d the leaf thickness, ϵ_l'' the complex part of the leaf dielectric constant, θ the observation elevation angle and the t_l expresses the single leaf transmissivity. It can be computed with the coherent model for layered media, discussed e.g. in Kong (1975). As input parameters the model requires the frequency, incidence angle, leaf thickness and ϵ_l. The leaf thickness distribution was manually measured and a mean value of approximately $d = 0.2$ mm was found. The leaf dielectric constant was determined with the semi-empirical model developed in Mätzler (1994a) that reads:

$$\epsilon_l = 0.522(1-1.32m_d)\epsilon_{sw} + 0.51 + 3.84m_d \quad (10)$$

with the leaf dry matter fraction m_d and the temperature dependent saline water dielectric constant ϵ_{sw}. This constant was determined with a dielectric model of sea water (Meissner & Wentz, 2004). For the salinity, we used a constant value of 0.5 ‰ which is a reasonable choice considering literature values given in Guglielmetti et al. (2007), McDonald et al. (2002) and El-Rayes and Ulaby (1987). In the latter report it is also seen that at X-band frequencies the influence of the salinity on the imaginary part of the dielectric constant is very low, therefore the assumption of a constant value does not hamper the applicability of the model. The quotient of the dried leaf mass and the fresh leaf mass m_d was determined to a value of about 0.4. In Mätzler (1994b) and Guglielmetti et al. (2007) the X-band opacity of a defoliated tree canopy was determined to values between 0.6 and 1.2. Since the visual impression suggests that our canopy under consideration consists of less branches than the canopies from the two cited articles, we set $\tau_b = 0.5$. This is also supported by the fact that our canopy is much younger wherefore the branches and the stem are less developed. A time series of the raw brightness temperature measurements as well as the results of this modeling and measuring approach are presented in Fig. 4.

The most prominent feature between the modeled and measured opacity time series is that they exhibit a strong anti-correlated behavior. Consequently, either the measurement or the opacity modeling was wrong or at least incomplete. Since the literature gives some indication that the dielectric constant of vegetation is related to the sapflow (McDonald et al., 2002), we hypothesized that the difference between the modeled and measured opacities originated from dielectric changes related to the sapflow in the observed trees, that were not accounted for in the model. In order to test this hypothesis, the time series of the difference between the modeled (τ_{temp}) and the measured opacity (τ_{meas}), formally written as

$$\tau_{\text{res}} = \tau_{\text{temp}} - \tau_{\text{meas}} \quad (11)$$

and named 'residual opacity', was plotted in Fig. 5-a in comparison to the time series of the sapflow.

We found a strong correlation between the two time series, at least during dry periods. Water on the leaves is expected to strongly influence the dielectric characteristics of the canopy, which is an effect that needs to be treated separately from the dielectric changes during dry conditions (see Section 3.3).

The interaction between the sapflow and τ_{res} can be quantified by only correlating the two variables during dry periods. For that, periods without water deposited on the leaves had to be identified. As a first criterion, the relative humidity, RH, had to be lower than 90%. This threshold was suggested by Thompson (1981) based on the common belief that plants remain wet after rain or dew as long as the relative humidity remains above 90% (Agam and Berliner, 2006). Although this is not a very sharp threshold visual inspection of our own data did not suggest the need to define a different threshold. The goal in our application was to reject cases where dew formation could potentially affect our interpretation. As a second criterion for dry periods, the delay after the latest detected rainfall had to be larger than 6 h such that there was enough time to evaporate the rain water intercepted in the tree canopy. In Fig. 6, a scatter plot between the dry residual opacity, $\tau_{\text{res}}^{\text{dry}}$, and the sapflow is shown.

The high correlation coefficient ($R^2 = 0.84$) supports the hypothesis of previously unaccounted dielectric changes induced by the flow of sap in the tree. With a linear model that relates the sapflow S with $\tau_{\text{res}}^{\text{dry}}$, determined as

$$\tau_{\text{res}}^{\text{dry}} = 1.29 \cdot S - 0.0367 \quad (12)$$

it was now possible to completely model the time series of the canopy opacity during dry periods. Hence, any deviations of the measured opacity to modeled opacity must originate from water in the canopy. Formally, this can be expressed as

$$\tau_{\text{meas}} = \tau_{\text{temp}} + \tau_{\text{res}}^{\text{dry}} + \tau_{\text{res}}^{\text{wet}}. \quad (13)$$

The opacity component that is due to a water film on the leaves, $\tau_{\text{res}}^{\text{wet}}$, is treated with some radiative transfer considerations that will be presented in more detail below.

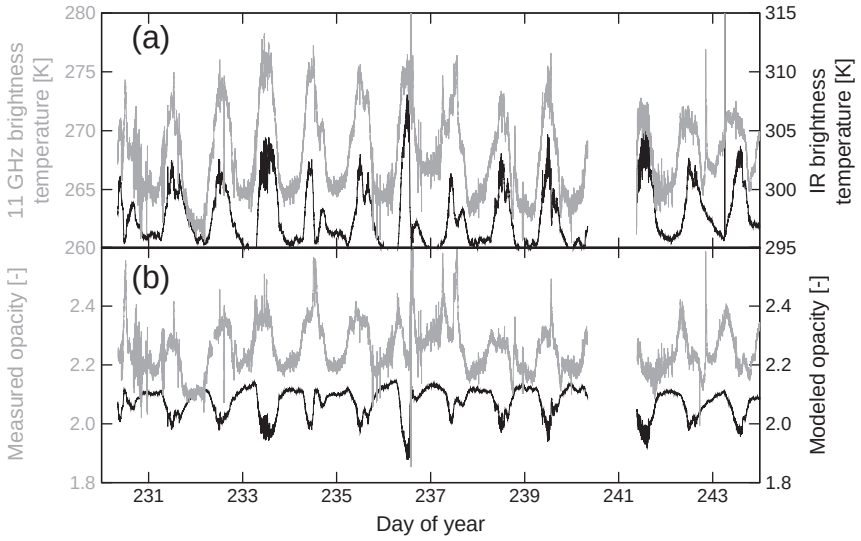

Fig. 4. a) Time series of the microwave and infrared brightness temperature measurements. b) Time series of the measured canopy opacity determined with Eqs. (2) and (3) and the result of the modeled opacity from Eq. (9).

3.3. Effect of wet leaves

In order quantify the influence of water on the leaves on the canopy opacity, the effective canopy opacity model from Eq. (9) has to be slightly modified. In our model, we considered the water as a homogeneous layer on both sides of the leaves. In the case of dew, this assumption is justified regarding the observations made by Kabela et al. (2009): The authors found that in a soybean and corn canopy, dew forms on top and on the bottom of the leaves, while the fraction between top- and bottom-formed dew depended not only on the dew amount but also on the time of the observation. For details, the reader is referred to Kabela et al. (2009). In the case of rain interception, we follow the assumption of a homogeneous water layer around the leaf by Schwank et al. (2008). The effect of such water layers on the single leaf transmissivity t_l is calculated with the matrix model of Bass et al. (1995). The second alteration in Eq. (9) concerns the leaf dielectric constant ϵ_l, as this is influenced by water-layer induced changes. Since we consider the water-leaf compound as stratified dielectric layers, the problem can be regarded as parallel plate capacitors connected in serial: The capacitance C of such a capacitor is calculated with the well-known formula

$$C = \frac{\epsilon A}{d} \tag{14}$$

with the plate area A, the dielectric constant of the medium between the plates ϵ and the plate distance d. Consequently, we can write the total capacity of serially connected capacitors with the water and leaf material acting as dielectric media as following:

$$\frac{d_w + d_l + d_w}{\epsilon_{\text{eff}} A} = \frac{d_w}{\epsilon_w A} + \frac{d_l}{\epsilon_l A} + \frac{d_w}{\epsilon_w A}. \tag{15}$$

Hereby, ϵ_w and ϵ_l are the dielectric constants of water and the leaf, respectively and $d_{w,\,l}$ are the corresponding thicknesses of the layers,

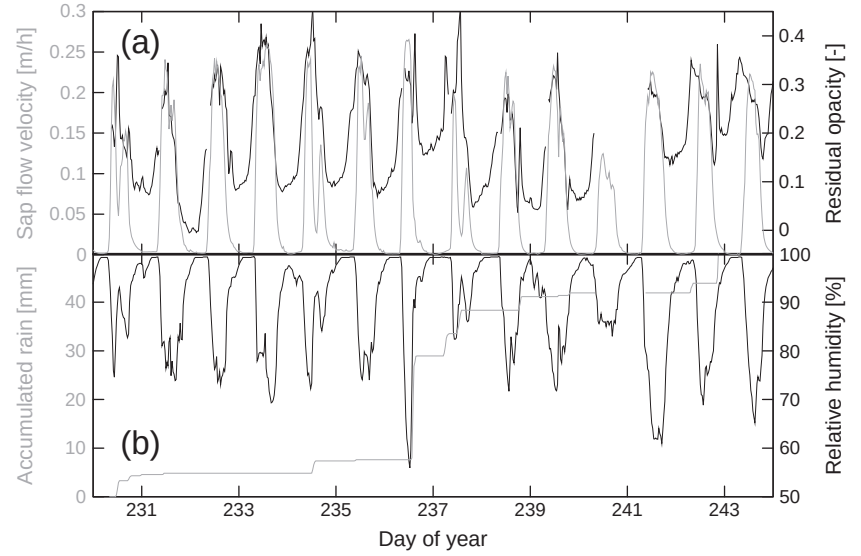

Fig. 5. a) Time series of the residual opacity τ_{res} and the sapflow of the trees. b) Time series of the rain accumulation and the relative humidity.

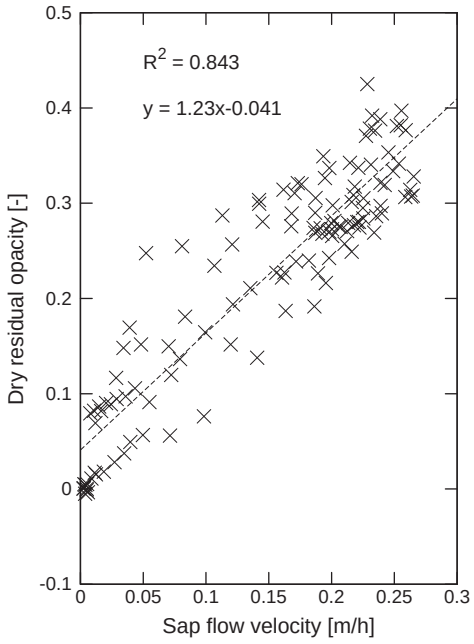

Fig. 6. Scatter plot of the sapflow versus τ_{res} during dry periods.

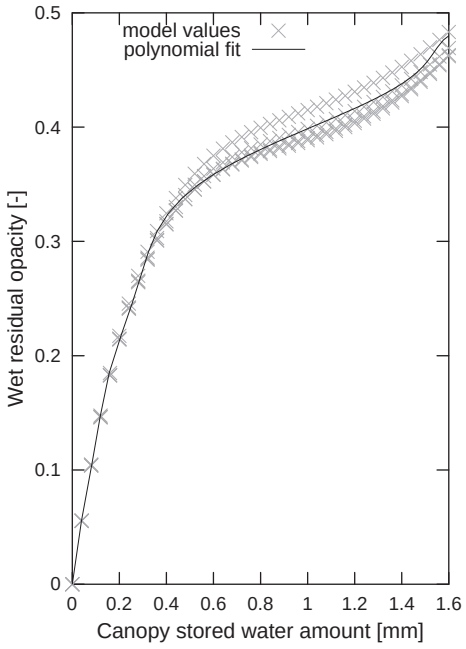

Fig. 7. Model result of the effect of water stored in the canopy (as a water film on both sides of the tree leaves) on the canopy opacity. The model was run at four temperatures between 290 and 300 K.

i.e. the distance of the capacitor plates. Since A is similar in all the terms the total dielectric constant can be written as:

$$\epsilon_{\text{eff}} = \frac{(2d_w + d_l)\epsilon_l\epsilon_w}{2d_w\epsilon_l + d_l\epsilon_w}. \tag{16}$$

By that, the thickness of the water layer can vary and we can observe the change in the opacity. The LAI enables us also to calculate the canopy stored water amount per unit area I:

$$I = 2 \cdot d_w \cdot \text{LAI} \tag{17}$$

Fig. 7 depicts the results of opacity calculations with different water layer thicknesses. In addition, the temperature was set to a range from 290 K to 300 K. These results were fitted with a polynomial of 9th degree, such that $\tau_{\text{res}}^{\text{wet}}$ can be directly related to the stored water amount in the canopy.

Separating $\tau_{\text{res}}^{\text{wet}}$ from the total observed opacity and transforming this variable into I by employing the determined relation between I and $\tau_{\text{res}}^{\text{wet}}$ enables us to quantitatively monitor time series of rain interception (I_{rain}) and dew formation I_{dew}. Hereby we assume the stored water amount in the canopy I to be a sum of rain interception and dew formation:

$$I = I_{\text{rain}} + I_{\text{dew}}. \tag{18}$$

Whether I_{dew} or I_{rain} (or both) contributes to I must be determined by observing the rain gage and the temperature of the canopy leaves relative to the dew point temperature.

Canopy water I_{rain} and I_{dew} can be quantified with even more accuracy if the knowledge of the occurrence of dry periods is used. During these periods, where I must be zero, an additive correction ΔI_{dry} is introduced which corrects the determined I to a value of zero, i.e., $\Delta I_{\text{dry}} = I$. For the whole time series, dry periods are determined with the criteria defined in Section 3.2 and ΔI_{dry} is calculated for all time points within these periods. The resulting ΔI_{dry} time series contains gaps at times when the conditions were wet. These gaps were finally filled with linear interpolation.

4. Results and discussion

4.1. Rain interception

With the methods developed in the previous section, the water stored in the canopy was quantified and the result is given in Fig. 8,

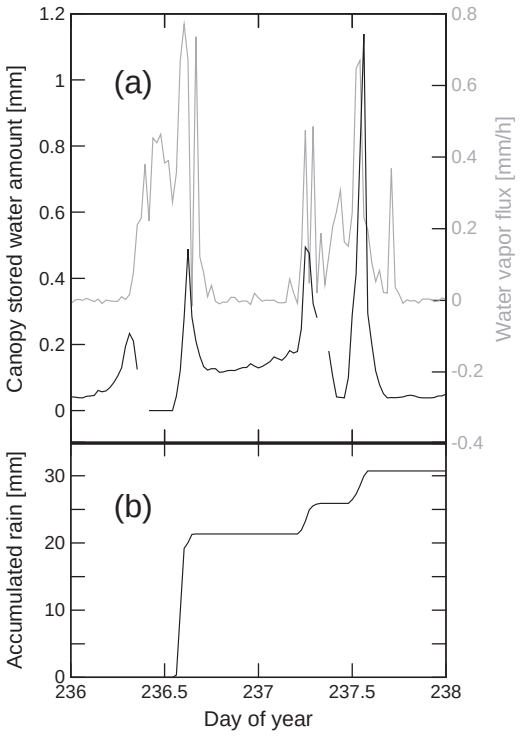

Fig. 8. a) 2-day time series of the canopy water storage I together with the above-canopy water vapor flux that was measured with the eddy covariance technique. b) Time series of the cumulative rainfall measured with a tipping bucket rain gage.

where a time series of I is plotted jointly with the above-canopy water vapor flux. We observe a temporal evolution of intercepted water and a first slight increase of I in the morning hours of day of year (DOY) 236. This increase did not correspond to any detected rain, and hence it is assumed that this signal is induced by dew formation which will be treated in more detail in Section 4.2. At the peak of the dew formation signal, the water vapor flux started simultaneously with sun rise and caused evaporation of dew from the leaves.

Shortly after midday of DOY 236, rainfall of high intensity started, immediately causing I to rise abruptly. At the same time, increasing water vapor fluxes were observed, which is most likely caused by direct evaporation of the intercepted water. After the rain stopped, I decreased quickly during about 2 h, but since the water vapor flux is more or less terminated after sun set, I does not reach zero causing some water to remain on the leaves during the night. Due to dew formation, I even slightly increases in the night hours until the two upcoming rain showers in the morning and the afternoon of DOY 237 again cause the water vapor flux as well as I to strongly increase. In between and after these rain events, strong evaporation reduces I to zero.

As can be seen in Fig. 8, it is not the most intense rain event that leads to the highest value of intercepted rain. The reason of this behavior might be related to possible inaccuracies of the modeled background brightness temperatures $T_{b,\mathrm{sky}}$, which is assumed to be more inaccurate during intense rain events. However, heavy precipitation also strongly disturbs the leaves which might facilitate the throughfall of rain through the canopy. In order to test the existence of a relationship between the rain intensity and the percentage of intercepted to total rainfall, all 13 rainfall events that occurred during the two week period from mid- to end of August have been analyzed and the results are plotted in Fig. 9. In this graph, the intercepted rain fraction was calculated by dividing the maximum amount of intercepted rain by the accumulated rain measured by the tipping bucket during each rain event, which was plotted as a function of the maximum rain intensity during each rain event.

We observe a strong anti-correlation between both quantities. For light rain events, up to 60% of rain was intercepted by the canopy while during intense precipitation, only about 4% of rain was intercepted by the canopy. During moderate events, i.e. rain intensities between 2 and 16 mm/h, the average interception percentage is 15%, which is in agreement with findings of Czikowsky and Fitzjarrald (2009) and Miralles et al. (2010).

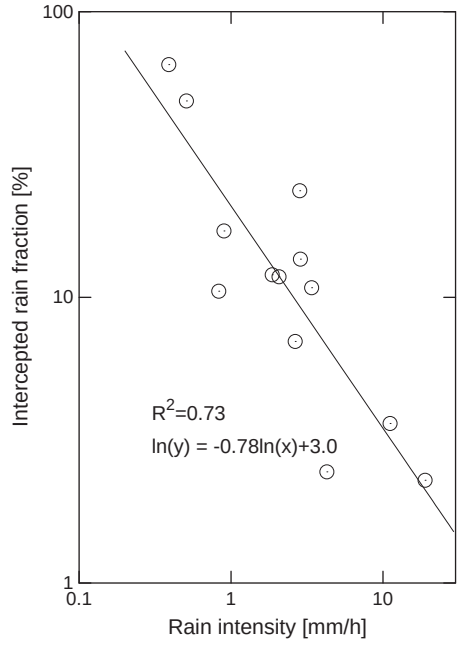

Fig. 9. The percentage of rain water intercepted in the canopy to the total rain amount as a function of the rain intensity.

4.2. Dew formation

While rain interception measurements can be performed with various techniques, the formation of dew on a forest canopy is much more difficult to quantify and very few (if any) direct measurements exist. As mentioned in Section 4.1 we believe that the increase of I during non-rainy nocturnal periods is induced by dew formation. A more evident understanding of this condensation process is obtained if several dry midnight to midday time series of I are averaged: The mean time series of 8 periods of similar kind is shown in Fig. 10 together with the averaged water vapor flux and the relative humidity. Although the standard deviation error bars are relatively large, distinct characteristics were observed: During the night, while the air around the canopy is saturated with water vapor, dew is deposited on the leaves and reaches a maximum at around 7.30 a.m. After sun rise (6.10 a.m.), the water vapor flux starts to increase at 7.00 a.m. with evolving turbulent mixing that reduces water vapor concentrations in the air surrounding the canopy. As soon as the air becomes unsaturated (between 7.30 a.m. and 8.00 a.m.), dew on the canopy starts to evaporate until the leaves are completely dry at around 11.00 a.m. In Fig. 10-b the averaged time series of the difference between the leaf temperature (measured with the infrared radiometer) and the temperature of the surrounding air is depicted. It is emphasized in the review paper by Agam and Berliner (2006) that, being a physical principle, dew only forms if the temperature of the respective surface (i.e. the leaves) is below the dew point. During the night hours of the time series shown in Fig. 10, the relative humidity is 100%, meaning that the physical temperature equals the dew point temperature. If then the leaf temperature is below the air temperature, dew can form on the leaf surface. The air–leaf temperature

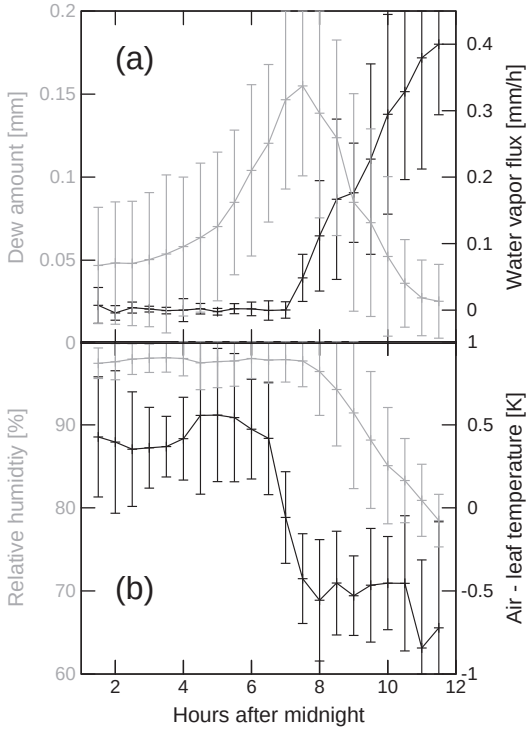

Fig. 10. a) Average over 8 time series of I and the water vapor flux that were not affected by rain. b) Relative humidity and the time series of the difference between the leaf temperature and the surrounding air temperature averaged over the same periods considered in panel a). The error bars in both plots show the standard deviation.

difference remains at a mostly steady and positive state during the night until 6.30 h. After sunrise (6.10 h), this difference starts to drop and reaches a new steady state at 8 h. In the transition phase between these two states, the water vapor flux is about to increase. In addition, dew also continuous to form and reaches its maximum amount shortly before the steady state is reached, which is most likely the time where the air–leaf temperature difference is becoming negative. It must be kept in mind that the absolute value of the air–leaf temperature difference might be slightly shifted towards higher values, since the leaf temperatures are inferred from IR radiation measurements that are likely to be affected by calibration errors and/or the fact that the tree canopy is not an optimal black body radiator.

Visual observations confirmed the measured duration of dew on the leaves. Due to the fact that this is the first time (to our knowledge) that the dew amount of a tree canopy is directly quantified, we cannot compare our findings with any references in the literature. However, since our rain interception measurements made with the same technique are in agreement with the findings of other authors (e.g. Czikowsky & Fitzjarrald, 2009) and since the averaged time series plotted in Fig. 10 seem realistic from the micro-meteorological point of view, we are confident that our measurements are reliable.

Furthermore, the ratio of dew amount to the total evaporated water enables some further insights: For the eight day period that was taken into account for the dew quantification, we calculated an average water vapor flux per day (3.24 mm) and related this value to the average maximum dew amount (0.17 mm). These figures show that a considerable fraction of 5.2% of the evaporated water vapor originates from the dew on the leaves.

5. Summary and conclusion

Diurnal cycles of downwelling microwave brightness temperatures were measured from below a 7 year old tropical tree plantation. The experimental setup was composed of a 11.4 GHz microwave and thermal infrared radiometer, an eddy covariance flux tower as well as xylem sapflow sensors that measured several trees in the close vicinity of the observed canopy. The radiometer was deployed on the ground and pointed at an elevation angle of 40° towards the canopy.

The canopy microwave opacity was calculated from modeled incoming sky brightness temperatures at 11.4 GHz and from thermal infrared temperatures that provided the physical temperature of the canopy. A canopy opacity model that considered the canopy temperature as the only input variable was found to be anti-correlated to the opacities that were inferred from microwave brightness temperature measurements. The difference between the modeled and the measured opacity during dry periods was found to be linearly related to the xylem sapflow of trees. Our study provides the first observation of a close relationship between the two variables. However, the physical cause of this behavior remains subject to speculation: on one hand, it is possible that the sapflow somehow modifies the dielectric constant of the plant material. On the other hand, sapflow is also expected to modify the water amount in the leaves: Under ample soil moisture conditions, xylem sapflow is increasing with decreasing leaf water status (Cermak et al., 1980) to compensate stomatal water loss.

The elucidated relation of the canopy opacity to the xylem sapflow made it possible to completely describe the opacity behavior during dry conditions. In addition, this enabled us to account for opacity changes that were caused by water deposited on the leaves of the canopy. The ability of taking into account a thin water film on both sides of the leaves was added to the canopy opacity model, leading to the possibility to quantitatively relate opacity changes to the amount of water stored in the canopy.

Time series of rain interception and of dew formation were calculated and it was found that between 4% and 60% percent of the rain amount was intercepted in the canopy, depending on the rain intensity. On average, about 15% of the rain amount was intercepted during rainfalls of medium intensities. By comparing the interception with the water vapor flux time series it was found that intercepted water is evaporated rapidly after it is deposited on the leaves, which resulted in an enhanced water vapor flux.

Our study provides the first direct measurements and quantifications of the temporal evolution of dew formation and evaporation in a tree canopy on a diurnal base. Dew accumulated during the night and until about 2 h after sunrise, when the water vapor flux began to exceed the dew formation rate. The dew continued to evaporate for another 3.5 h until the surface of the leaves was completely dry. The fact that dew continued to form even after sunrise can be explained with the Priestly–Taylor equilibrium equation (Priestley & Taylor, 1972), which is used to estimate the actual evaporation. In this equation, evaporation is linear to the difference between net radiation and the soil heat flux. Measurements made by Clothier et al. (1986) show that this difference is very small after sunrise and starts to increase significantly 1 h after sunrise. However, this time delay between sunrise and the beginning of evaporation most probably depends on the location as well as the structure and type of the canopy and is therefore only qualitatively comparable to our findings.

Acknowledgments

Since this project was based on a private initiative, the first author is grateful for the financial support from the following Swiss institutions: Prof. Heinrich Greinacher Foundation, Bern; Travel grants commission and the Remote sensing commission of the Swiss Academy of Sciences SCNAT; Institute of Plant, Animal and Agroecosystem Sciences, ETH Zurich; Institute of Applied Physics, University of Bern. He is also indebted to his wife Fabienne Zeugin for constant support during the time in Panama. We would like to thank Catherine Potvin and the administrative staff of the Smithsonian Tropical Research Institute, Panama, who made this project possible by providing access to the research plantation and by logistics support. Furthermore, thanks go to the Institute of Geography, University of Bern, that lent the hemispherical camera, one anonymous reviewer for his detailed and helpful comments and last but not least to José and Iliana Monteza-Cabrera with family who shared their home and became essential for the success of the project. S. Wolf and W. Eugster acknowledge financial support from the North–South Centre (former Swiss Centre for International Agriculture) of ETH Zurich. N. Kunert acknowledges financial support from the German Research Foundation (grant Ho-2119/3-1).

References

Agam, N., & Berliner, P. (2006). Dew formation and water vapor adsorption in semi-arid environments—A review. *Journal of Arid Environments*, *65*, 572–590.

Bass, M., Stryland, E. V., Williams, D., & Wolfe, W. (1995). Optical properties of films and coatings, Part 11. *Handbook of Optics*. New York, San Francisco, Washington D.C.: McGraw-Hill.

Bouten, W., Schaap, M., & Vermetten, A. (1996). Monitoring and modelling canopy water storage amounts in support of atmospheric deposition studies. *Journal of Hydrology*, *181*, 305–321.

Bouten, W., Swart, P., & Water, E. D. (1991). Microwave transmission, a new tool in forest and hydrological research. *Journal of Hydrology*, *124*, 119–130.

Cermak, J., Huzula, J., & Penka, M. (1980). Water potential and sap flow rate in adult trees with moist and dry soil as used for the assessment of root system depth. *Biologia Plantarum*, *22*, 34–41.

Chukhlantsev, A. A. (2006). *Microwave radiometry of vegetation canopies*. 3300 AA Dordrecht, The Netherlands: Springer.

Clothier, B., Clawson, K., P. P., Jr., Moran, M., Reginato, R., & Jackson, R. (1986). Estimation of soil heat flux from net radiation during the growth of alfalfa. *Agricultural and Forest Meteorology*, *37*, 319–329.

Czekala, H., Crewell, S., Simmer, C., Thiele, A., Hornbostel, A., & Schroth, A. (2001). Interpretation of polarization features in ground-based microwave observations as caused by horizontally aligned oblate raindrops. *Journal of Applied Meteorology*, *40*, 1918–1932.

Czikowsky, M., & Fitzjarrald, D. (2009). Detecting rainfall interception in an Amazonian rain forest with eddy flux measurements. *Journal of Hydrology*, *377*, 92–105.

Della Vecchia, A., Ferrazzoli, P., Wigneron, J. -P., & Grant, J. P. (2007). Modeling forest emissivity at L-band and a comparison with multitemporal measurements. *IEEE Geoscience and Remote Sensing Letters*, *4*, 508–512.

El-Rayes, M., & Ulaby, F. T. (1987). Microwave dielectric behavior of vegetation material. *Tech. rep., Radiation Laboratory, Department of Electrical Engineering and Computer Science, The University of Michigan*.

Eugster, W., & Senn, W. (1995). A cospectral correction model for measurement of turbulent NO2 flux. *Boundary-Layer Meteorology*, *74*(4), 321–340.

Ferrazoli, P., & Guerriero, L. (1996). Passive microwave remote sensing of forests: A model investigation. *IEEE Transactions on Geoscience and Remote Sensing*, *34*, 433–443.

Flores, E. M., & Marin, W. A. (2003). *Tabebuia rosea* (Bertol.) DC. In J. A. Vozzo (Ed.), *Tropical tree seed manual. Part II—Species descriptions. Agriculture Handbook*, *721*. (pp. 737–739) Washington, DC: United States Department of Agriculture, Forest Service.

Fournier, L. A. (2003). *Anacardium excelsum* (Bertero & Balb. ex Kunth) Skeels. In J. A. Vozzo (Ed.), *Tropical tree seed manual. Part II—Species descriptions. Agriculture Handbook*, *721*. (pp. 294–296) Washington, DC: United States Department of Agriculture, Forest Service.

Granier, A. (1985). A new method of sap flow measurement in tree stems. *Annals of Forest Science*, *42*, 193–200.

Granier, A. (1987). Evaluation of transpiration in a Douglas-fir stand by means of sap flow measurements. *Tree Physiology*, *3*, 309–320.

Guglielmetti, M., Schwank, M., Mätzler, C., Oberdörster, C., Vanderborght, J., & Flühler, H. (2007). Measured microwave radiative transfer properties of a deciduous forest canopy. *Remote Sensing of Environment*, *109*(4), 523–532.

Han, Y., & Westwater, E. R. (2000). Analysis and improvement of tipping calibration for ground-based microwave radiometers. *IEEE Transactions on Geoscience and Remote Sensing*, *38*, 1260–1276.

Holliday, P. (1980). *Fungus diseases of tropical crops.* Cambridge, England: Cambridge University Press.

Janssen, M. A. (1993). An introduction to the passive microwave remote sensing of atmospheres. In M. A. Janssen (Ed.), *Atmospheric remote sensing by microwave radiometry* (pp. 1–35). New York: Wiley.

Kabela, E. D., Hornbuckle, B. K., Cosh, M. H., Anderson, M. C., & Gleason, M. L. (2009). Dew frequency, duration, amount, and distribution in corn and soybean during SMEX05. *Agricultural and Forest Meteorology*, *149*, 11–24.

Karam, M. A., Amar, F., Fung, A. K., Mougin, E., Lopes, A., Le Vine, D. M., et al. (1995). A microwave polarimetric scattering model for forest canopies based on vector radiative transfer theory. *Remote Sensing of Environment*, *53*, 16–30.

Kidron, G., Barzilay, E., & Sachs, E. (1965). Microclimate control upon sand microbiotic crusts, western Negev Desert, Israel. *Geomorphology*, *36*, 1–18.

Kimmins, J. (1973). Some statistical aspects of sampling throughfall precipitation in nutrient cycling studies in British Columbian coastal forests. *Ecology*, *54*, 1008–1019.

Kong, J. A. (1975). *The theory of electromagnetic waves.* New York: J. Wiley & Sons.

Kunert, N., unpublished data. Specific leaf area of the trees in the experimental plantation in Sardinilla, Panama.

Kunert, N., Schwendenmann, L., & Holscher, D. (2010). Seasonal dynamics of tree sap flux and water use in nine species in Panamanian forest plantations. *Agricultural and Forest Meteorology*, *150*, 411–419.

Kurum, M., Lang, R. H., Neill, P. E., Joseph, A. T., Jackson, T. J., & Cosh, M. H. (2009). L-band radar estimation of forest attenuation for active/passive soil moisture inversion. *IEEE Transactions on Geoscience and Remote Sensing*, *47*, 3026–3040.

Lawrence, D., Thronton, P., Oleson, K., & Bonan, G. (2007). The partitioning of evapotranspiration into transpiration, soil evaporation, and canopy evaporation in a GCM: Impacts on land–atmosphere interaction. *Journal of Hydrometeorology*, *8*, 862–880.

Liebe, H. J., Hufford, G. A., & Cotton, M. G. (1993). Propagation modeling of moist air and suspended water/ice particles at frequencies below 1000 GHz. *AGARD 52nd Specialists Meeting Electromagn. Wave Propagation Panel. Palma de Mallorca, Spain*.

Mätzler, C. (1994a). Microwave (1 − 100 GHz) dielectric model of leaves. *IEEE Transactions on Geoscience and Remote Sensing*, *32*, 947–949.

Mätzler, C. (1994b). Microwave transmissivity of a forest canopy: Experiments made with a beech. *Remote Sensing of Environment*, *48*, 172–180.

McDonald, K. C., Zimmermann, R., & Kimball, J. S. (2002). Diurnal and spatial variation of xylem dielectric constant in Norway spruce (*Picea abies* [l.] Karst.) as related to microclimate, xylem sap flow, and xylem chemistry. *IEEE Transactions on Geoscience and Remote Sensing*, *40*, 2063–2082.

Meissner, T., & Wentz, F. J. (2004). The complex dielectric constant of pure and sea water from microwave satellite observations. *IEEE Transactions on Geoscience and Remote Sensing*, *42*, 1836–1849.

Miralles, D. G., Gash, J. H., Holmes, T. R. H., de Jeu, R. A. M., & Dolman, A. J. (2010). Global canopy interception from satellite observations. *Journal of Geophysical Research*, *115*, D16122.

Moreau, M., Testud, J., & Le Bouar, E. (2009). Rainfall spatial variability observed by X-band weather radar and its implication for the accuracy of rainfall estimates. *Advances in Water Resources*, *32*, 1011–1019.

Noffsinger, T. (1965). Survey of techniques for measuring dew. In A. Waxler (Ed.), *Humidity and moisture* (pp. 523–531). New York: Reinhold.

Pampaloni, P. (2004). Radiometry of forests. *Waves in Random Media*, *14*, 275–298.

Potvin, C., & Dutilleul, P. (2009). Neighborhood effects and size-asymmetric competition in a tree plantation varying in diversity. *Ecology*, *90*, 321–327.

Priestley, C., & Taylor, R. (1972). On the assessment of surface heat flux and evaporation using large-scale parameters. *Monthly Weather Review*, *100*, 81–92.

Rosenkranz, P. W. (1998). Water vapor microwave continuum absorption: A comparison of measurements and models. *Radio Science*, *33*, 919–928.

Sandi, C., & Flores, E. M. (2003). *Hura crepitans*. In J. A. Vozzo (Ed.), *Tropical tree seed manual. Part II—Species descriptions. Agriculture Handbook*, *721*. (pp. 511–513) Washington, DC: United States Department of Agriculture, Forest Service.

Santi, E., Paloscia, S., Pampaloni, P., & Pettinato, S. (2009). Ground-based microwave investigations of forest plots in Italy. *IEEE Transactions on Geoscience and Remote Sensing*, *47*, 3016–3025.

Satake, M., & Hanado, H. (2004). Diurnal change of Amazon rain forest σ^0 observed by Ku-band spaceborne radar. *IEEE Transactions on Geoscience and Remote Sensing*, *42*, 1127–1134.

Schneebeli, M., & Mätzler, C. (2011). A radiative transfer model for an idealized and non-scattering atmosphere and its application for ground-based remote sensing. *Journal of Quantitative Spectroscopy and Radiative Transfer*, *112*, 883–892.

Schneebeli, M., Wolf, S., Eugster, W., & Mätzler, C. (2008). X-Band opacity of a tropical tree canopy and its relation to intercepted rain, eddy fluxes and other meteorological variables. *2008 Microwave Radiometry and Remote Sensing of the Environment*. Italy: Florence.

Schwank, M., Guglielmetti, M., Mätzler, C., & Flühler, H. (2008). Testing a new model for the L-band radiation of moist leaf litter. *IEEE Transactions on Geoscience and Remote Sensing*, *46*, 1982–1994.

Thompson, N. (1981). The duration of leaf wetness. *Meteorological Magazine*, *110*, 1–12.

Valente, F., David, J. S., & Gash, J. H. C. (1997). Modelling interception loss for two sparse eucalypt and pine forests in central Portugal using reformulated Rutter and Gash analytical models. *Journal of Hydrology*, *190*, 141–162.

Vrugt, J., Dekker, S., & Bouten, W. (2003). Identification of rainfall interception model parameters from measurements of throughfall and forest canopy storage. *Water Resources Research*, *39*(9).

Way, J., Paris, J., Dobson, M., McDonald, K., Ulaby, F. T., & Vanderbilt, V. (2004). Diurnal change in trees as observed by optical and microwave sensors: The EOS synergism study. *IEEE Transactions on Geoscience and Remote Sensing*, *29*(6), 817–820.

Webb, E., Pearman, G., & Leuning, R. (1980). Correction of flux measurements for density effects due to heat and water-vapor transfer. *Quarterly Journal of the Royal Meteorological Society*, *106*(447), 85–100.

Wegmüller, U., Mätzler, C., & Njoku, E. G. (1995). Canopy opacity models. In E. G. Njoku, P. Pampaloni, B. J. Choudhury, & Y. H. Kerr (Eds.), *Passive microwave remote sensing of land–atmosphere interactions* (pp. 375–387). Utrecht, The Netherlands: VSP.